J. Hydrau., Coast. Environ. Eng., JSCE, No. 740/II-64, 197-208, 2003 August

TWO-DIMENSIONAL BEHAVIOR OF A STRONG BORE OVER A SLOPING BEACH

Hideo MATSUTOMI

Member of JSCE, Dr. Eng., Associate Professor, Dept. of Civil and Environmental Eng., Akita University
(1-1, Tegata Gakuen-cho, Akita 010-8502, Japan)

Physical and numerical experiments are carried out to clarify several fundamental characteristics of the two-dimensional behavior of a strong bore over a sloping beach, which has been observed to be caused by a tsunami. An approximate method (referred to as "a ray theory for bores" in this paper) is presented to analyze the two-dimensional behavior of bores. The analyses with the use of the method proposed in this study and Snell's law show that the behavior of strong bores over sloping beaches is quite different from that of waves.

Key Words: *strong bore, two-dimensional behavior, physical and numerical experiments, tsunami*

1. INTRODUCTION

Edge bores were witnessed, photographed and videotaped on the north Akita coast in Japan at the time of the 1983 Nihonkai-Chubu earthquake tsunami, and Shuto[1] emphasized the necessity of studying edge bores from a viewpoint of tsunami disaster prevention.

It is well known that a tsunami causes edge waves over a sloping beach. Thus, many studies have been conducted on edge waves generated by tsunamis (for example, Carrier & Noiseux[2], Koshimura et al.[3], Fujima et al.[4]). However, there are few studies on edge bores including experimental studies.

Chen[5] conducted a forerunning study on edge bores over sloping beaches through physical experiments with solitary waves. The experiments were carried out for beaches with a slope steeper than tan20°. He pointed out the formation of a horizontal eddy with a vertical axis in the neighborhood of the shoreline but mainly focused on the classification of edge bores. The two-dimensional behavior of a bore right off the horizontal eddy, which would play an important role in its formation and shape, was not mentioned at all. Subsequently, Uda et al.[6] carried out physical experiments on edge bores over a gently sloping beach. However, they did not take up the two-dimensional behavior of a bore over a sloping beach, either.

Most sandy beaches have slopes much milder than tan20°, and tsunamis often break and form bores over such gently sloping beaches. The two-dimensional behavior of a bore over such a beach, caused by a tsunami, seems to affect not only the bore height but also the incident angle of the bore to the shoreline, and ultimately, the size and form of the edge bore. Therefore, it is important, from the viewpoint of tsunami disaster prevention, to examine the fundamental characteristics of the two-dimensional behavior of a bore over a sloping beach, and to develop a relatively simple method, compared with existing numerical simulation methods[7], of analyzing the fundamental two-dimensional behavior of such a bore, particularly bore propagation directions, i.e., bore rays, without setting the troublesome moving shoreline boundary condition or being affected by a run-up bore.

In light of the above circumstances, in this study, we aim, in the first phase, to examine several fundamental characteristics of the two-dimensional behavior of a strong bore, caused by a tsunami, over a sloping beach through both physical and numerical experiments, and to develop an approximate method of analyzing the fundamental two-dimensional behavior of such a bore. Analyses of both bore behavior by the developed method and wave behavior based on Snell's law are also carried out to elucidate the difference between the two-dimensional behaviors of strong bores and waves.

2. EXPERIMENTS

(1) Physical experiments[8),9)]

The experimental flume is schematically shown in **Fig.1**. The flume is 100 cm wide, 10 cm high and 350

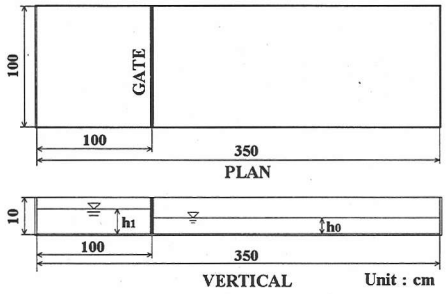

Fig.1 Experimental flume.

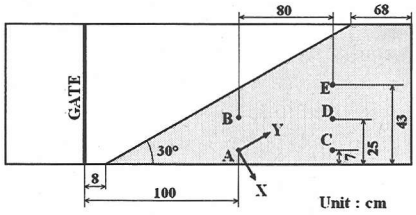

(a) Uniformly sloping bottom

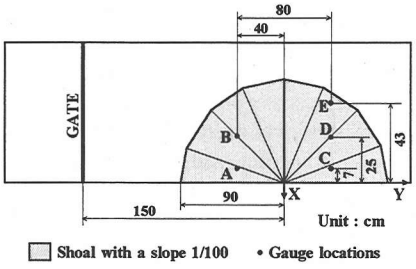

(b) Conical shoal

Fig.2 Bottom models.

cm long with a horizontal bed, and is made of transparent vinyl chloride. Strong bores are generated by rapidly pulling up a gate, made of brass 0.2 cm thick, installed 1 m from one end of the flume. Two configurations of the sea bottom with a slope of 1/100, made of transparent vinyl chloride 0.4 cm thick are modeled inside the flume, as shown in **Figs.2** (a) and (b). A sea bottom with a slope of 1/25 made of clay is set up in each case so as to smoothly connect the sloping bottom with the horizontal bottom. One configuration is a uniformly sloping bottom and the other is a conical shoal. They are fully submerged in water. Capacitance-type wave gauges are installed at locations A ~ E shown in **Figs.2** (a) and (b), to measure time histories of the incoming bore surface elevation. Their arrangement is the same in both cases.

Experimental conditions and results are summarized in **Tables 1** and **2**, where h_1 is the initial water depth in the upstream region of the gate, h_0 is the constant water depth in

Table 1 Experimental conditions and results (uniformly sloping bottom).

h_1 (cm)	h_0 (cm)	s	α_0 (°)	ΔH_A (cm)	ΔH_B (cm)	ΔH_C (cm)	ΔH_D (cm)	ΔH_E (cm)	ΔT_E (s)
7				2.070	2.064	2.127	1.971	1.788	-.0016
8	2	0.01	60	2.408	2.410	2.434	2.253	2.089	.0002
9				2.802	2.790	2.755	2.580	2.406	.0055

Table 2 Experimental conditions and results (conical shoal).

h_1 (cm)	h_0 (cm)	s	α_0 (°)	ΔH_A (cm)	ΔH_B (cm)	ΔH_C (cm)	ΔH_D (cm)	ΔH_E (cm)	ΔT_E (s)
7				2.111	2.068	1.906	1.892	1.765	.0125
8	2	0.01	90	2.458	2.418	2.196	2.158	2.041	.0201
9				2.777	2.712	2.384	2.376	2.332	.0279

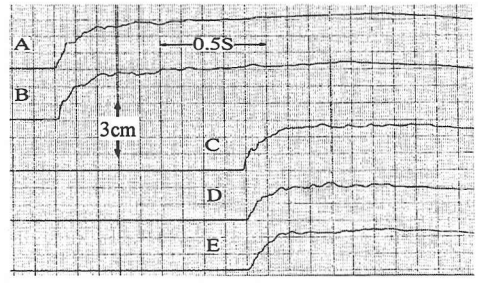

(a) Conical shoal (h_p=0.8 cm)

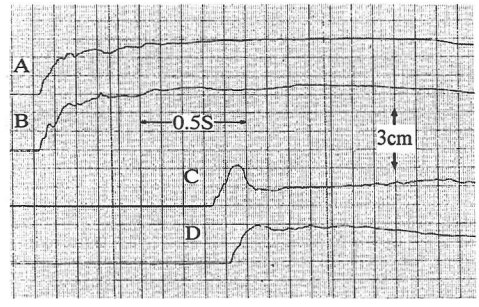

(b) Conical island (h_p< 0)

Fig.3 Time histories of bore surface elevation (h_1=9 cm, h_0=2 cm).

the downstream region of the gate, s is the bottom slope, α_0 is the initial incident angle of the bore, ΔH is the bore height, the subscripts A ~ E accompanying the bore height denote the locations where the bore heights are measured and ΔT_E is the time-lag between the propagation of the bore from B to D and from A to C. The still water depth h_p at the top of the conical shoal (which is the origin of the coordinate system (X, Y) shown in **Fig.2** (b)) is fixed at 0.8 cm.

Ten runs were performed under each experimental condition. The experimental results listed in **Tables 1** and **2** are averages of those ten runs. It is difficult to determine the bore height from data recorded on the papers because of the ambiguity of the definition of the bore height (see **Fig.3** (a)). Therefore, the average bore surface elevation between 0.3 and 0.4 s after the arrival of the bore front at each measurement point is adopted as the bore height. The standard de-

viation of bore heights is smaller than 4.3 % of the average bore height in all cases. Positive values of ΔT_E imply that the bore takes longer to travel from B to D than from A to C. It can be concluded from the data in the tables that strong bores over a sloping bottom tend to turn their propagation direction to the deep-water side and to decrease their bore height further offshore.

Figure 3 (a) shows representative time histories of the surface elevation of a bore over the conical shoal. The length scale in the figure is rough because it is slightly different at each measurement point. Since the experimental scale is small, it is difficult to identify the trend of the bore travel time difference from the figure at a glance. To clarify the time difference, another experiment is carried out under the condition that h_1 and h_0 are the same as those in **Fig.3** (a), but part of the section A-C is not submerged (conical island, h_p<0). The shoreline between the sections A-C and B-D was built up by increasing the slope of the conical shoal. **Figure 3** (b) shows the result and clearly indicates that the bore propagation velocity on the shallow-water side is higher than that on the deep-water side.

(2) Numerical experiments

To avoid the difficult problem of the moving shoreline boundary condition, numerical experiments are carried out only for bores propagating over the conical shoal described in **§ 2 (1)**. The results of the numerical experiments are indicated as "the computed" results below and used only for qualitative discussions of bore behavior.

a) Governing equations

The following conventional depth-integrated nonlinear shallow-water equations are adopted as the governing equations:

$$\frac{\partial h}{\partial t}+\frac{\partial P}{\partial X}+\frac{\partial Q}{\partial Y}=0, \tag{1}$$

$$\frac{\partial P}{\partial t}+\frac{\partial}{\partial X}\left(\frac{P^2}{h}\right)+\frac{\partial}{\partial Y}\left(\frac{PQ}{h}\right)+gh\frac{\partial h}{\partial X}=-s_X gh-f\frac{P\sqrt{P^2+Q^2}}{h^2}, \tag{2}$$

$$\frac{\partial Q}{\partial t}+\frac{\partial}{\partial X}\left(\frac{PQ}{h}\right)+\frac{\partial}{\partial Y}\left(\frac{Q^2}{h}\right)+gh\frac{\partial h}{\partial Y}=-s_Y gh-f\frac{Q\sqrt{P^2+Q^2}}{h^2}, \tag{3}$$

where t is the time, X and Y are the fixed horizontal coordinates, h is the water depth, P and Q are the flow rates per unit width in the X and Y directions, g is the acceleration due to gravity, s_X and s_Y are bottom slopes in the X and Y directions and f is a friction factor.

b) Numerical scheme

The sidewall on the deep-water side in **Fig.2** (b) is moved by 30 cm to widen the computational domain and so that there is the conical shoal with s=1/100 everywhere. The sidewall on the shallow-water side is removed to make the computational domain symmetric in the X direction (-130 cm $\le X \le$ 130 cm) and to avoid trivial difficulties in the computations. The computational domain is discretized with a staggered grid of fixed sizes (ΔX, ΔY). The sizes are ΔX=ΔY=1 cm in all computations.

As a consequence of the above-mentioned grid, the staggered leap-frog scheme is adopted to discretize the governing equations, except for the convective terms to which the up-wind scheme is applied. Therefore, the numerical scheme has first-order accuracy, and is popular for tsunami numerical simulations (see the reference 10 for details).

c) Initial conditions

The water is set to be quiescent in the whole domain, except in the vicinity of the gate where Ritter[11] and Stoker[12] solutions for the dam-break problem are applied.

The Stoker solution offers a constant water depth and flow rate while the Ritter solution offers transitional ones as expressed as follows:

$$h=\frac{1}{9g}\left(2\sqrt{gh_1}-\frac{Y}{t}\right)^2, \tag{4}$$

$$Q=\frac{2}{27g}\left(\sqrt{gh_1}+\frac{Y}{t}\right)\left(2\sqrt{gh_1}-\frac{Y}{t}\right)^2. \tag{5}$$

The water depth at t=11.5Δt and flow rate at t=12Δt are given, where Δt is the time interval in the computations. $\Delta Y/\Delta t$=400 cm/s is fixed, which fully satisfies the Courant-Friedrichs-Lewy condition.

d) Front condition

The propagation of the bore front is calculated explicitly with the use of the bore propagation velocity one step before. More concretely speaking, the bore front is propagated in the Y direction at the Y-directional bore propagation velocity ($\ge$ the bore propagation velocity).

Figures 4 (a) ~ (e) show the expected bore front trajectories on the Y-t plane. The solid and broken lines show the grids for the flow rate and the water depth, respectively. I is the time step and JS is the spatial step just behind the bore front for both the flow rate and the water depth. The circles, squares and triangles denote the water depth, and the flow rates in the X and Y directions respectively. The filled symbols denote variables already known and the open symbols denote unknowns.

The unknowns on the left-hand side of the thick broken line with arrow heads at both ends are determined by solving the difference equations based on the numerical schemes described in **§ 2 (2) b)**. The unknowns on the right-hand side are determined by assuming that (1) the water surface in the Y direction behind the bore front is horizontal, (2) the water particle velocity in the Y direction behind the bore front is dependent only on the time, and (3) Q (I+1, JS-2)=Q (I+1, JS-1) in the cases shown in **Figs.4** (a) ~ (c). In addition, we apply the following conventional bore condition just at the bore front:

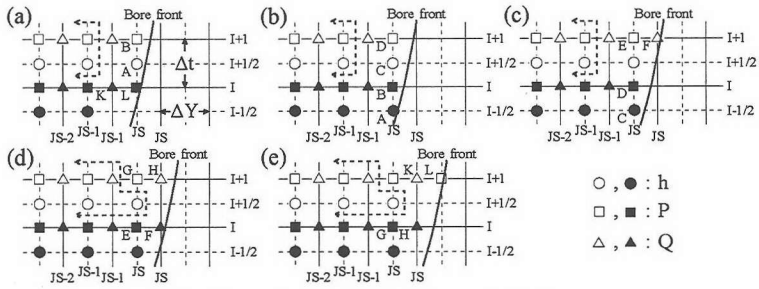

Fig.4 Expected trajectories of bore front on the *Y-t* plane.

$$\xi = \sqrt{\frac{gh_f}{2h_{0f}}(h_f + h_{0f})}, \qquad (6)$$

where ξ is the bore propagation velocity, and h_f and h_{0f} are the water depth at the bore front and the quiescent water depth before the bore front, respectively. Therefore, the front condition does not satisfy the mass conservation law strictly.

e) Boundary condition

The flow rates in the direction perpendicular to the vertical sidewall boundary of the computational domain are set equal to zero.

3. APPROXIMATE METHOD

The two-dimensional behavior over an arbitrary beach topography cannot be elucidated through numerical computation even for a linear wave subjected to Snell's law. An approximate method that is relatively simple compared with existing numerical simulation methods and that belongs to the same category as Snell's law in the sense that there are numerical errors and they can give bore or wave rays directly is developed to analyze the fundamental two-dimensional behavior of a strong bore over a sloping beach without setting the troublesome moving shoreline boundary condition or being affected by a run-up bore. The results by this approximate method are indicated as "the calculated" results below.

(1) Governing equations

Figures 5 and **6** show the coordinate systems, beach topography, bore model and definition of symbols. The (*X*, *Y*) coordinate system is fixed to the beach and the (*x*, *y*) coordinate system to the bore front.

Let us consider a strong bore caused by a tsunami with a long wave period and assume the following.

(1) The pressure is hydrostatic.

(2) The water ahead of the bore is undisturbed.

(3) The inclination δ of the water surface in the bore propagation direction (*x* direction) is constant.

(4) The water particle velocities u (*x* direction) and v (*y* direction) are independent of both x and y, i.e., $u(t)$ and $v(t)$.

(5) The spatial distribution of bore height $\Delta H(y, t)$ is linear in the bore model.

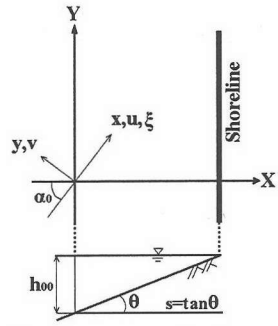

Fig.5 Coordinate systems and beach topography.

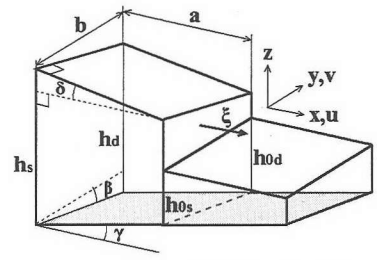

Fig.6 Bore model and definition of symbols.

The assumption (3) is equivalent to specifying some of the incident tsunami conditions. The velocity $v(t)$ is the average in the y cross section because it must be zero at the bore front.

The mass, and *x*- and *y*-direction momentum conservation laws based on the above assumptions are as follows:

$$\frac{dM}{dt} = \frac{\rho b}{2}(h_s + h_d)u - \frac{\rho b}{2}(h_s + h_d - h_{0s} - h_{0d} - 2a\tan\gamma - 2a\tan\delta)\xi + \rho a(h_s - h_d)v, \qquad (7)$$

$$\frac{dP_M}{dt} = \frac{\rho b}{2}(h_s + h_d)u^2 - \frac{\rho b}{2}(h_s + h_d - 2a\tan\gamma - 2a\tan\delta)u\xi + \rho a(h_s - h_d)uv + \frac{\rho g b}{6}\{(h_s^2 + h_s h_d + h_d^2) - (h_{0s}^2 + h_{0s}h_{0d} + h_{0d}^2)\} - \rho g V\tan\gamma - \rho f a b u\sqrt{u^2 + v^2}, \qquad (8)$$

$$\frac{dQ_M}{dt} = \rho a(h_s - h_d)v^2 + \frac{\rho b}{2}(h_s + h_d)uv$$
$$-\frac{\rho b}{2}(h_s + h_d - 2a\tan\gamma - 2a\tan\delta)v\xi$$
$$+\frac{\rho g a}{2}\{h_s^2 - a(h_s - h_d)(\tan\gamma + \tan\delta) - h_d^2\}$$
$$+\rho g V\tan\beta - \rho f abv\sqrt{u^2+v^2}, \quad (9)$$

where M, P_M and Q_M are the mass, and x- and y-direction momentums in the control volume defined as the volume of the offshore hexahedron shown in **Fig.6**, ρ is the density of water, a and b are the constant length and width of the control volume, h_s and h_d are the water depth on the right- and left-hand sides at the rear of the control volume, h_{0s} and h_{0d} are the quiescent water depth on the right- and left-hand sides at the front of the control volume, V is the control volume and the subscript y denotes a differentiation with respect to y. These equations have the accuracy of $O(a, b)$.

Tan γ and tan β are the beach slopes in the bore propagation and bore front line directions, respectively. Each has the following relation to the beach slope s (=tan θ) and incident angle α of the bore in the fixed (X, Y) coordinate system:

$$\tan\gamma = s\cos\alpha, \qquad \tan\beta = s\sin\alpha. \quad (10)$$

Since $M=\rho V$, $P_M=Mu$ and $Q_M=Mv$, Eqs. (7) ~ (9) can be rewritten as follows:

$$\frac{dV}{dt} = f_1(V, u, v, \xi, V_y)$$
$$= bh_{rc}u - b(h_{fc} - h_{0fc})\xi - vV_y, \quad (11)$$

$$\frac{du}{dt} = f_2(V, u, v, \xi, V_y)$$
$$= -\frac{bh_{0fc}u\xi}{V} + \frac{gb}{6V}\left(3h_{rc}^2 + \frac{V_y^2}{4a^2} - 4h_{0fc}^2 + h_{0s}h_{0d}\right)$$
$$-g\tan\gamma - f\frac{abu\sqrt{u^2+v^2}}{V}, \quad (12)$$

$$\frac{dv}{dt} = f_3(V, u, v, \xi, V_y)$$
$$= -\frac{bh_{0fc}v\xi}{V} - \frac{gV_y}{ab} + g\tan\beta - f\frac{abv\sqrt{u^2+v^2}}{V}, \quad (13)$$

where the following symbols are introduced:

$$h_{rc} = \frac{h_s + h_d}{2} = h_{fc} + a(\tan\gamma + \tan\delta)$$
$$= \frac{V}{ab} + \frac{a}{2}(\tan\gamma + \tan\delta),$$

$$h_{0fc} = \frac{h_{0s} + h_{0d}}{2} = h_{0s} + \frac{b}{2}\tan\beta = h_{0d} - \frac{b}{2}\tan\beta,$$

$$V_y = a(h_d - h_s).$$

h_{rc} is the water depth at the center of the rear of the control volume, and h_{fc} and h_{0fc} are the water depth and quiescent water depth at the center of the front of the control volume respectively. When α=0, Eqs. (11) ~ (13) become those derived by Matsutomi[13].

At this stage, the number of governing equations is three and that of unknown variables is five: V, u, v, ξ and V_y. Two more governing equations are necessary to close the present problem. A governing equation for V_y can be obtained by differentiating Eq. (11) with respect to y:

$$\frac{dV_y}{dt} = f_4(u, \xi, V_y)$$
$$= \frac{V_y u}{a} + b\left(-\frac{V_y}{ab} + \tan\beta\right)\xi, \quad (14)$$

where the second derivative of V with respect to y is set equal to zero under the assumption (5).

The last governing equation is for the bore propagation velocity ξ. The conventional bore condition must be unconditionally satisfied at the bore front, i.e., it never has an explicit term of bottom friction and is expressed in the present model as follows:

$$\xi = f_5(V; V_y)$$
$$= \sqrt{\frac{gh_{fc}}{6h_{0fc}}\frac{(3h_{fc}^2 + V_y^2/4a^2 - 4h_{0fc}^2 + h_{0s}h_{0d})}{(h_{fc} - h_{0fc})}}. \quad (15)$$

Equations (11) ~ (14) are simultaneously solved by the 4th-order Runge-Kutta method, and then Eq. (15) is used to determine a new value of ξ.

(2) Initial conditions

As the initial distribution of bore height $\Delta H(y, 0) = \Delta H_0$ is generally given, it can be considered that the initial values of V, V_y and ξ are known.

There are no steady bores that obliquely propagate over a sloping beach. However, it can be assumed that the time change rate of the dependent variables is sufficiently small in the offshore region. Setting Eqs. (12) and (13) equal to zero, the water particle velocities u and v can be approximated as

$$u = \frac{g}{h_{0fc}\xi}\left\{\frac{1}{6}\left(3h_{rc}^2 + \frac{V_y^2}{4a^2} - 4h_{0fc}^2 + h_{0s}h_{0d}\right)\right.$$
$$\left. -\frac{V}{b}\tan\gamma\right\}, \quad (16)$$

$$v = \frac{gV}{bh_{0fc}\xi}\left(\tan\beta - \frac{V_y}{ab}\right), \quad (17)$$

where the friction terms are also ignored.

Equations (16) and (17) are adopted as the initial values of u and v. When the bore height is constant in the y direction, v is obviously zero.

(3) Calculation procedure

No special techniques are used in the calculations, except in the determination of the bore propagation direction.

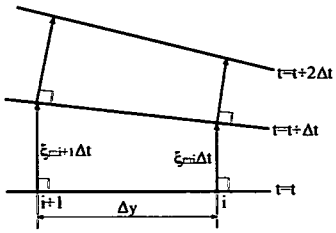

Fig.7 Estimation of bore propagation direction.

Table 3 Calculation conditions.

	a (cm)	b (cm)	Δt (s)	Δy (cm)	s	α_0 (°)	δ (°)	f
Sloping beach	1	1	.0001	1	0.01	60	0	0
Conical shoal	1	1	.0001	1	0.01	90	0	0

The calculations are carried out simultaneously at two points initially Δy apart on the y axis, and the bore propagation direction is geometrically determined as shown in **Fig.7**.

The calculation procedure is as follows.

(1) Give the beach slope s, length a and width b of the control volume, initial spatial interval Δy between the two calculation points i and i+1, initial incident angle α_0 of the bore, initial bore height ΔH_0 and inclination δ of the water surface.

(2) Determine the initial values of V, u, v, ξ and V_y by the method described in **§ 3 (2)**.

(3) Determine new values of V, u, v and V_y after Δt by solving Eqs. (11) ~ (14) simultaneously, where Δt is the time interval in the calculations.

(4) Determine a new value of ξ by substituting the new values of V, u, v and V_y into Eq. (15).

(5) Determine the average value ξ_m of the bore propagation velocity for Δt, and then propagate the bore front by $\xi_m \Delta t$ at right angles to the bore front line at each calculation point (see **Fig.7**).

(6) Regard the straight line passing through new bore front positions as the new bore front line and the direction perpendicular to the straight line as the new bore propagation direction.

(7) Reiterate procedures (3) ~ (6) using the newly determined values of the dependent variables to propagate the bore.

Unless stated otherwise, the values shown in **Table 3** are adopted in the calculations.

4. RESULTS AND DISCUSSIONS

(1) Performance of the approximate method

Calculations are carried out under the conditions of s=1/100, α_0=0°, δ=0° and f=0 to test the performance of the developed method described in **§ 3**, through comparison with the numerical results obtained by Keller et al.[14]

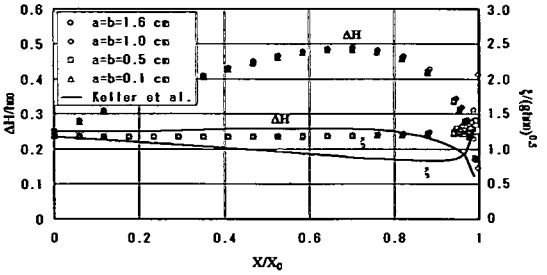

(a) $\Delta H_0/h_{00}$=0.25

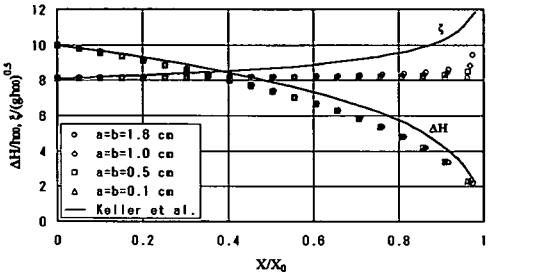

(b) $\Delta H_0/h_{00}$=10

Fig.8 Comparisons of results obtained by Keller et al. and the approximate method over a uniformly sloping beach (α_0=0°).

Figures 8 (a) and (b) show the results obtained by Keller et al. and by using the approximate method for the dimensionless bore height $\Delta H/h_{00}$ and bore propagation velocity $\xi/\sqrt{gh_{00}}$ respectively, where ΔH is the local bore height, h_{00} (=1.6 cm) is the still water depth at the origin of the X axis (see **Fig.5**), i.e., at the starting point of the bore, and X_0 is the distance from the origin to the shoreline. The solid lines are the results obtained by Keller et al. under the condition of a uniform bore incidence to X=0. The plotted symbols are the results of the approximate method. For reference, four sets of (a, b) were selected in the calculations. The set where a=b=1.6 cm corresponds to the spatial grid size ΔX adopted by Keller et al. under the present conditions of h_{00} and s.

Figure 8 (a) indicates that if an incident bore is weak, the approximate method gives much larger values for both the bore height and bore propagation velocity compared with those reported by Keller et al. This is due to the assumptions (3) and (4) in **§ 3 (1)**, because, in reality, the water particle velocity u behind the bore front decreases and its decreasing rate is higher than the increasing rate of the surface elevation in the case of a weak bore as shown by Keller et al.[14], i.e., the approximate method overestimates the flow rate behind the bore front. These results suggest that the approximate method does not perform well in the case of weak bores because the assumption δ=0° is not valid any more.

On the other hand, **Fig.8** (b) indicates that if an incident

bore is strong enough, the approximate method gives almost the same results as Keller et al.'s. This suggests that the approximate method is of practical use in analyzing the two-dimensional behavior of a strong bore over a sloping beach.

Strictly speaking, in **Fig.8** (b), Keller et al.'s results are slightly large compared with those of the approximate method, and the difference between their bore propagation velocities is slightly large compared with that between their bore heights. The former is due to the fact that the decreasing rate of the water particle velocity behind the bore front is lower than the increasing rate of the surface elevation in the case of a strong bore as shown by Keller et al.[14], i.e., the approximate method underestimates the flow rate behind the bore front, which suggests that it is necessary to adopt $\delta>0°$. The latter seems to be mainly due to the fact that Eq. (6) for the bore propagation velocity has a tendency to emphasize the bore height difference $\Delta H_K - \Delta H_A$ in the shallower region than $h_{00}/2$ as seen from the following expression:

$$\frac{\xi_K-\xi_A}{\sqrt{gh_{00}}}=\sqrt{\frac{h_{fK}^2}{2h_{00}h_{0f}}\left(1+\frac{h_{0f}}{h_{fK}}\right)}-\sqrt{\frac{h_{fA}^2}{2h_{00}h_{0f}}\left(1+\frac{h_{0f}}{h_{fA}}\right)}$$
$$\approx\sqrt{\frac{h_{00}}{2h_{0f}}}\,\frac{\Delta H_K-\Delta H_A}{h_{00}}$$

where the subscripts K and A denote the results obtained by Keller et al. and of the approximate method respectively, and $\Delta H_K=h_{fK}-h_{0f}$ and $\Delta H_A=h_{fA}-h_{0f}$ are used after Taylor expansion in the derivation of the expression.

(2) Propagation

a) Uniformly sloping beach

Figures 9 (a) and (b) show the calculated bore front trajectories over the uniformly sloping bottom shown in **Fig.2** (a), where Y is the axis parallel to the shoreline, X is that perpendicular to Y, and they have their origin at the location A or B. In these figures, "9-2", for example, denotes h_1=9 cm and h_0=2 cm, and "R-K" is the abbreviation for the 4th-order Runge-Kutta method. The experimental results of ΔH_A and ΔH_B shown in **Table 1** are adopted as the initial conditions of the bore. The wave front trajectory derived from Snell's law is also shown by the solid line with crosses, which is expressed as follows[15]:

$$Y=\frac{h_{00}}{s\sin^2\alpha_0}\left\{\alpha_0-\sin^{-1}\left(\sin\alpha_0\sqrt{1-\frac{sX}{h_{00}}}\right)\right\}+\frac{h_{00}}{s\sin\alpha_0}\cdot$$
$$\left\{\sqrt{1-\frac{sX}{h_{00}}}\sqrt{1-\left(1-\frac{sX}{h_{00}}\right)\sin^2\alpha_0}-\cos\alpha_0\right\}. \qquad (18)$$

Figures 9 (a) and (b) indicate that strong bores over a uniformly sloping beach have a tendency to turn their propagation direction to the deep-water side, unlike waves, and the distribution of bore height in the y direction affects the bore propagation direction. The former trend is the same as the measurement described in **§ 2 (1)**.

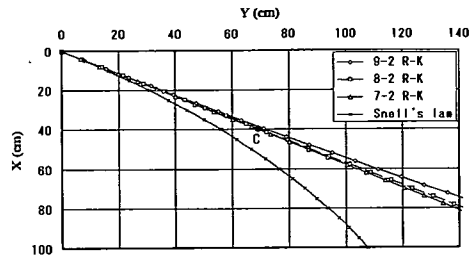

(a) Section A-C

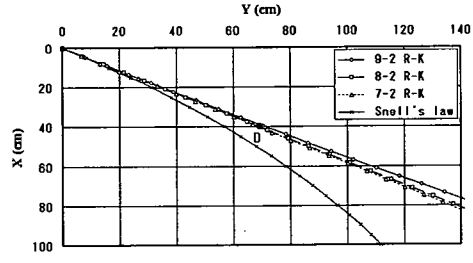

(b) Section B-D

Fig.9 Bore front trajectories and Snell's law over a uniformly sloping beach (α_0=60°).

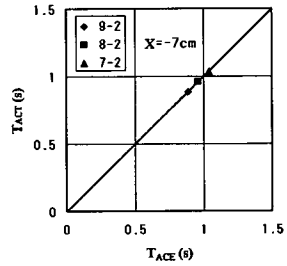

(a) Travel time (section A-C)

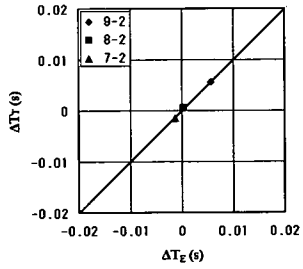

(b) Travel time difference

Fig.10 Comparisons of measured and calculated results over a uniformly sloping beach (α_0=60°).

The calculated trajectories pass the close vicinity of the location C or D. This implies that no interpolation of the measured results is needed for comparisons between the measured and calculated results described below.

Figures 10 (a) and (b) show the measured and calculated results of the travel time T_{AC} of the bore from A to C

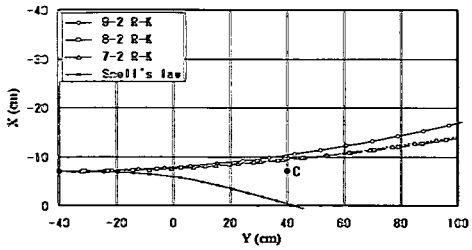

(a) Section A-C

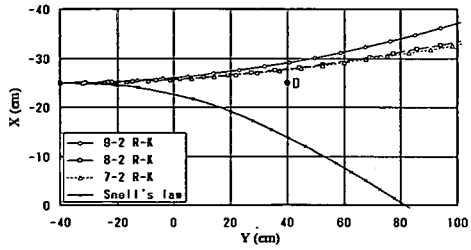

(b) Section B-D

Fig.11 Bore front trajectories and Snell's law over a conical shoal (α_0=90°).

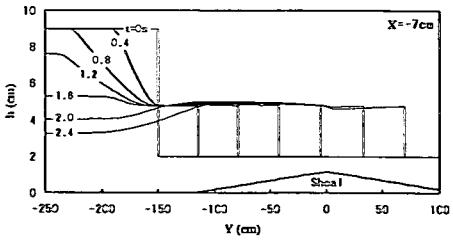

(a) Bore surface profile (section A-C)

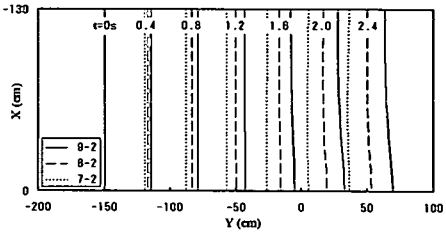

(b) Bore front line

Fig.13 Computed spatial distributions over a conical shoal.

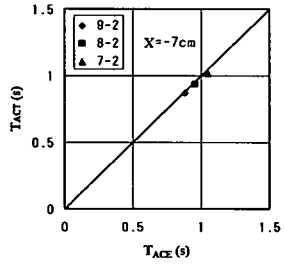

(a) Travel time (section A-C)

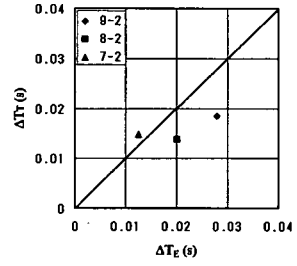

(b) Travel time difference

Fig.12 Comparisons of measured and calculated results over a conical shoal (α_0=90°).

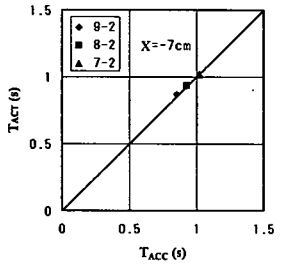

(a) Travel time (section A-C)

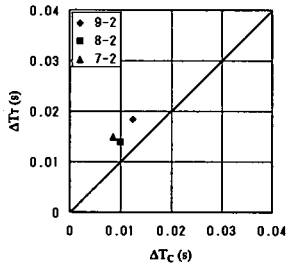

(b) Travel time difference

Fig.14 Comparisons of computed and calculated results over a conical shoal (α_0=90°).

and the time-lag ΔT between the propagation of the bore from B to D and from A to C over the uniformly sloping beach respectively, where the subscripts E and T accompanying T_{AC} and ΔT denote the measured and calculated results, respectively. It can be understood from the figures that the agreement is surprisingly good for both items.

b) Conical shoal

Figures 11 (a) and (b) show the calculated bore front trajectories over the conical shoal (see **Fig.2** (b) for the coordinates and legend). The result derived from Snell's law is also shown by the solid line with crosses, which was obtained by numerically solving the following equation[16]:

$$\frac{d\alpha}{dr} = \frac{1}{r\sqrt{(sr_0 + h_{00})r^2/(sr + h_{00})r_0^2 \sin^2\alpha_0 - 1}}, \quad (19)$$

where $r = \sqrt{X^2 + Y^2}$ is the radius with the origin at the top of the conical shoal and r_0 is the distance from the origin to the starting point of the bore. Equation (19) is also solved by the 4th-order Runge-Kutta method.

Figures 11 (a) and (b) indicate that the trend of the change of the bore propagation direction is the same as that over the uniformly sloping bottom, but the calculated trajectories pass significantly far from the location C or D. The latter suggests that it is necessary to interpolate the measured results to compare with the calculated results. This is the reason why the measurement point E is adopted. The measured results are adjusted by linear interpolation between the locations C and D for the cases shown in **Fig.11** (a) or D and E for the cases shown in **Fig.11** (b).

Figures 12 (a) and (b) show the measured and calculated results of the travel time T_{AC} of the bore from A to C and the time-lag ΔT between the propagation of the bore from B to D and from A to C over the conical shoal, respectively. It can be understood from the figures that the agreement between them is good even in the case of the conical shoal.

Figures 13 (a) and (b) show the computed spatial distributions of the bore surface profile and bore front line every 0.4 s over the conical shoal, respectively. Bottom friction is ignored in the computations. **Figure 13** (a) shows the case of h_1=9 cm and X=-7 cm (section A-C), and indicates that a weak hydraulic jump is formed after the bore front passes the top of the conical shoal. **Figure 13** (b) clearly indicates faster propagation of the bore front on the shallow-water side. This is consistent with positive values of ΔT in both the measurements and the calculations as shown in **Fig.12** (b), which also imply faster propagation of the bore front on the shallow-water side.

Figures 14 (a) and (b) show the computed and calculated results of the travel time T_{AC} of the bore from A to C and the time-lag ΔT between the propagation of the bore from B to D and from A to C over the conical shoal, respectively, where the subscript C accompanying T_{AC} and ΔT denotes the computed results. Although the computed results have a tendency to be slightly small compared with the calculated, i.e., the computed bore fronts propagate faster than the calculated, the agreement between them is good for both items. The faster propagation seems to be mainly due to the horizontal water surface and constant flow rate, i.e., a kind of extrapolation in the front condition under the assumptions (1) and (3) in **§ 2 (2) d)**, which give larger values for both the bore front height and flow rate than the actual values.

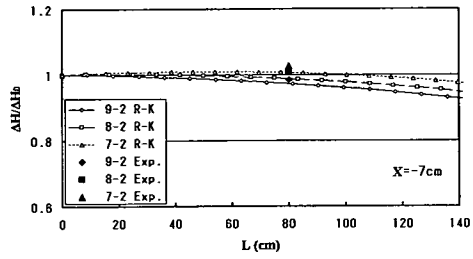

a) Section A-C

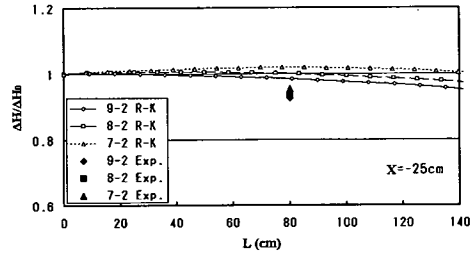

(b) Section B-D

Fig.15 Comparisons of measured and calculated amplification factors over a uniformly sloping beach (α_0=60°).

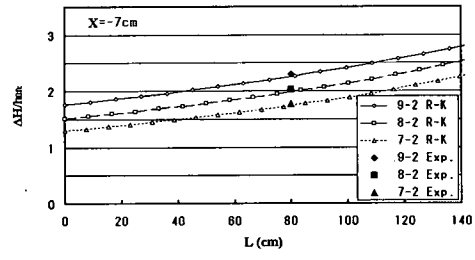

(a) Section A-C

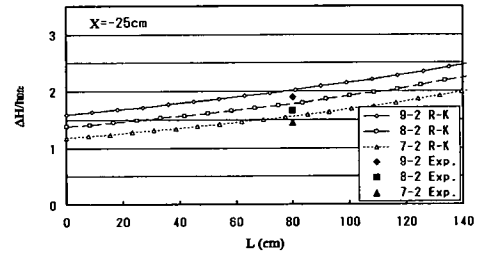

(b) Section B-D

Fig.16 Comparisons of measured and calculated relative bore heights over a uniformly sloping beach (α_0=60°).

(3) Amplification factor and relative bore height

a) Uniformly sloping beach

Figures 15 (a) and (b) show the measured and calculated bore height amplification factors $\Delta H/\Delta H_0$ over the uniformly sloping beach, where L is the distance from the starting point of the bore along a bore front trajectory and "Exp." denotes the measured results. The measured results are larger than those calculated in **Fig.15** (a) despite

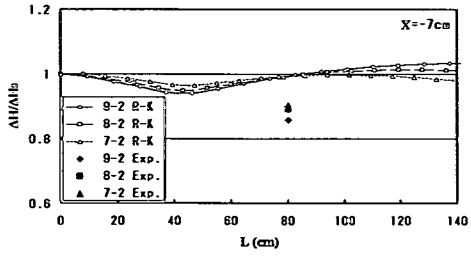

(a) Section A-C

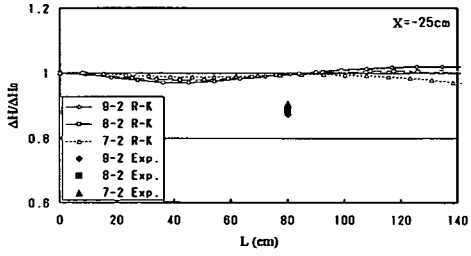

(b) Section B-D

Fig.17 Comparisons of measured and calculated amplification factors over a conical shoal (α_0=90°).

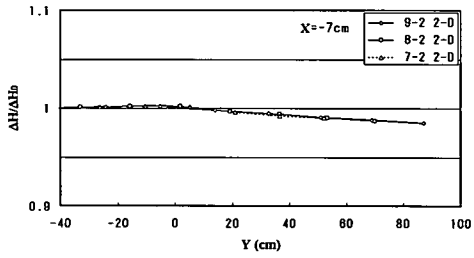

(a) Section A-C

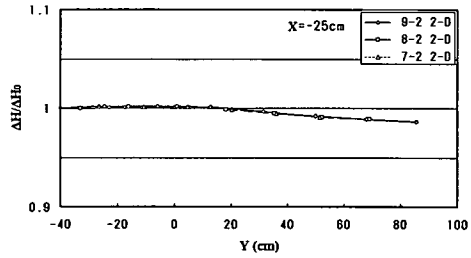

(b) Section B-D

Fig.18 Computed amplification factors over a conical shoal (α_0=90°).

neglecting bottom friction in the calculations. This seems to be due to the ambiguity of the definition of the bore height in the physical experiments (see **Fig.3** (a)). However, it can be concluded from the figures that the agreement between them is fairly good in both cases.

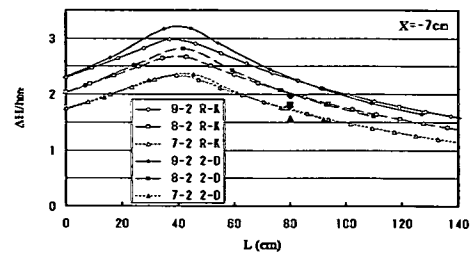

(a) Section A-C

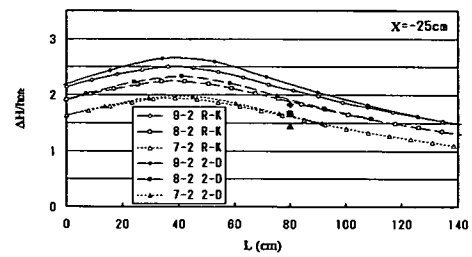

(b) Section B-D

Fig.19 Comparisons of measured, calculated and computed relative bore heights over a conical shoal (α_0=90°).

Figures 16 (a) and (b) show the measured and calculated relative bore heights $\Delta H/h_{0fc}$ over the uniformly sloping beach. The trend that the measured are slightly large in section A-C and are small in section B-D is the same as that in the case of amplification factor.

b) Conical shoal

Figures 17 (a) and (b) show the measured and calculated bore height amplification factors over the conical shoal. The calculated results clearly indicate one of the characteristics of strong bores[14], i.e., the bore height decreases over an ascending bottom (0 cm $\leq L \leq$ 40 cm). The agreement between them is poor in both cases. This seems to suggest that bottom friction must be taken into account.

Figures 18 (a) and (b) show the computed bore height amplification factors over the conical shoal, where "2-D" denotes the computed results. It must be noted that the abscissa is not L but Y (L is related to Y as $L=\int_0^Y \xi\, dt \approx Y$+40 cm) and the ordinate is magnified in the figures. The trend is different from that calculated shown in **Fig.17**, i.e., the amplification factors increase slightly over the ascending bottom in all cases. This also seems to be due to the front condition adopted in the computations, and leads to the result that the computed bore fronts propagate faster than the calculated ones, as stated in the discussion of **Fig.14**.

Figures 19 (a) and (b) show the measured, calculated and computed relative bore heights over the conical shoal, where the same marks as used before are adopted for the measured results. Strictly speaking, the abscissa for the computed results is Y, which has a tendency to give larger values than the measured and calculated ones around the

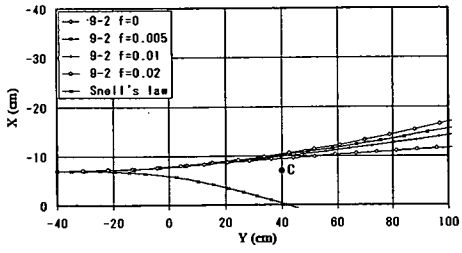

(a) Trajectory

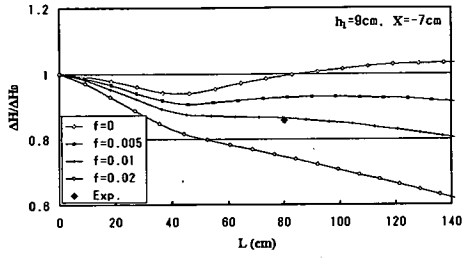

(b) Amplification factor

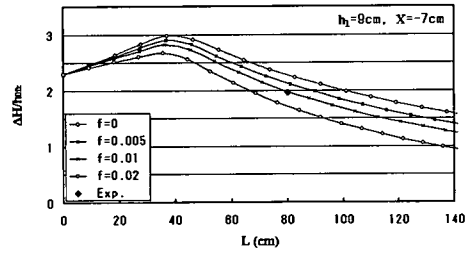

(c) Relative bore height

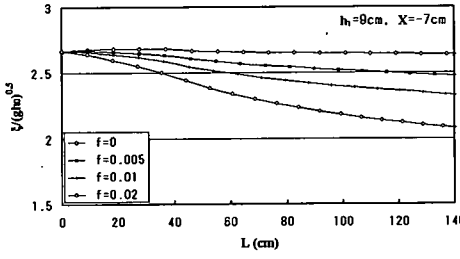

(d) Propagation velocity

Fig.20 Influences of bottom friction upon a bore over a conical shoal (α_0=90°).

top of the conical shoal. The agreement between the measured and other results is poor in both cases. This also suggests that it is important to take account of bottom friction to predict the behavior of a strong bore.

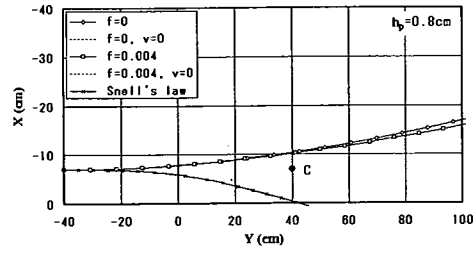

(a) h_p=0.8 cm

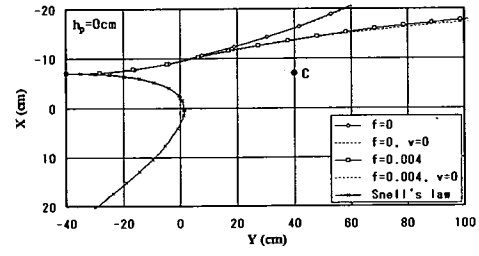

(b) h_p=0 cm

Fig.21 Influence of v upon bore front trajectory over a conical shoal (α_0=90°).

(4) Influence of bottom friction

Figures 20 (a) ~ (d) show the influences of bottom friction on the bore front trajectory, bore height amplification factor, relative bore height and bore propagation velocity, respectively. The measured amplification factor and relative bore height are again shown using the same marks as before. The results correspond to the case that h_1=9 cm and X=-7 cm (section A-C), and suggest that the behavior of a strong bore is significantly affected by bottom friction.

The friction factor f ($\approx gn^2/h_{fc}^{1/3}$) in the physical experiments is deduced to be about 0.004, where n is Manning's roughness coefficient. If this friction factor is adopted, the measured amplification factors and relative bore heights can be fairly well predicted by the approximate method. However, there is still an appreciable difference between the measured and predicted results. This seems to be mainly because the bore model is based on the long wave approximation. The effect of nonhydrostatic pressure distribution cannot be ignored in reality.

(5) Influence of water particle velocity v

Figures 21 (a) and (b) show examples of the influence of water particle velocity v upon the bore front trajectory over the conical shoal, where "v=0" means that v is ignored in the calculations. **Figure 21** (a) shows the case that h_p=0.8 cm, h_1=9 cm and X=-7 cm (section A-C). **Figure 21** (b) shows a hypothetical case that h_p=0 cm, but the height and its distribution of the initial bore and the friction factor are the same as those in **Fig.21** (a). In conclusion, the influence of v upon the bore front trajectory, i.e., upon the behavior of

a strong bore is small under realistic circumstances in the present bore model. As h_p tends to 0, however, the influences of both ν and bottom friction increase.

5. CONCLUSIONS

We obtained the following main results:

(1) An approximate method that might be called "a ray theory for bores" was developed to analyze the two-dimensional behavior of a strong bore, caused by a tsunami, over a sloping beach. The validity of the method was confirmed through comparison with the results obtained by Keller et al. and both physical and numerical experiments although the method has a tendency to underestimate the bore propagation velocity.

(2) Through the analyses of both bore behavior by the approximate method and wave behavior based on Snell's law, it was shown that strong bores over sloping beaches behaved differently from waves.

(3) The two-dimensional behavior of a strong bore over a sloping beach is significantly affected by bottom friction.

ACKNOWLEDGMENTS: This study was carried out during the author's stay in University of Bristol as an overseas research fellow of the Ministry of Education, Culture, Sports, Science and Technology of Japan. The author wishes to thank Professor D. H. Peregrine, Department of Mathematics, University of Bristol, for his helpful comments during this study.

REFERENCES

1) Shuto, N.: The Nihonkai-Chubu earthquake tsunami on the North Akita Coast, *Coastal Eng. in Japan*, JSCE, Vol. 28, pp. 255-264, 1985.

2) Carrier, G. F. and Noiseux, C. F.: The reflection of obliquely incident tsunamis, *JFM*, Vol. 133, pp. 147-160, 1983.

3) Koshimura, S., Imamura, F. and Shuto, N.: Propagation of obliquely incident tsunamis on a slope Part 1: Amplification of tsunamis on a continental slope, *Coastal Eng. Jour.*, JSCE, Vol. 41, No. 2, pp. 151-164, 1999.

4) Fujima, K., Dozono, R. and Shigemura, T.: Generation and propagation of tsunami accompanying edge waves on a uniform sloping shelf, *Coastal Eng. Jour.*, JSCE, Vol. 42, No. 2, pp. 211-236, 2000.

5) Chen, T. C.: Experimental study on the solitary wave reflection along a straight sloped wall at oblique angle of incidence, *US Beach Erosion Board Tech. Memo.*, No. 124, 24 p., 1961.

6) Uda, T., Omata, A., Tsuji, Y. and Kajiura, K.: Experiments and theory on bores, *Report on a special study of natural disasters supported by the Grant-in Aid for Scientific Research from the Ministry of Education, Science and Culture*, Edited by Shuto, N., No. A-63-1, Chap. 4, pp. 87-140, 1988. (in Japanese)

7) For example, Bokhove, O., Patterson, M. D. and Peregrine, D. H.: Breaking shallow water wave simulations in the surf and swash zone, *Proc. 27th ICCE*, ASCE, Vol. 1, pp. 720-732, 2000.

8) Matsutomi, H., Mochizuki, A. and Sato, N.: Laboratory experiments on the propagation of an obliquely incident bore over a uniformly sloping beach, *Tohoku Journal of Natural Disaster Science*, Vol. 36, pp. 237-240, 2000. (in Japanese)

9) Matsutomi, H. and Mochizuki, A.: Behavior of a bore over a conical shoal, *Tohoku Journal of Natural Disaster Science*, Vol. 37, pp. 67-73, 2001. (in Japanese)

10) Goto, C. and Ogawa, Y.: Numerical method of tsunami simulation with the staggered leap-frog scheme, Dept. of Civil Eng., Faculty of Eng., Tohoku University, 52 p., 1982. (in Japanese)

11) Ritter, A.: Die fortpflanzung der wasserwellen, *Zeitschrift des Vereines Deutscher Ingenieure* (Berlin), Vol. 36, Pt. 2 No. 33, pp. 947-954, 1892.

12) Stoker, J. J.: The formation of breakers and bores, *Communications on Pure and Applied Mathematics*, Vol. 1, pp. 1-87, 1948.

13) Matsutomi, H.: On the propagation of a bore over a sloping beach, *Coastal Eng. in Japan*, JSCE, Vol. 28, pp. 45-58, 1985.

14) Keller, H. B., Levine, D. A. and Whitham, G. B.: Motion of a bore over a sloping beach, *JFM*, pp. 302-316, 1960.

15) Sayama, J., Goto, C. and Shuto, N.: Errors induced by refraction in tsunami numerical simulation, *Proc. of Coastal Eng.*, JSCE, Vol. 33, pp. 201-205, 1986. (in Japanese)

16) Arthur, R. S.: Refraction of water waves by island and shoals with circular bottom-contours, *Transactions*, AGU, Vol. 27, No. 2, pp. 168-177, 1946.

(Received February 26, 2002)